HHS Public Access

Author manuscript

Acta Biomater. Author manuscript; available in PMC 2016 September 15.

Published in final edited form as:

Acta Biomater. 2015 September 15; 24: 117–126. doi:10.1016/j.actbio.2015.06.010.

Aligned multilayered electrospun scaffolds for rotator cuff tendon tissue engineering

Steven B. Orr[a], **Abby Chainani**[a,b], **Kirk J. Hippensteel**[a], **Alysha Kishan**[a,b], **Christopher Gilchrist**[a], **N. William Garrigues**[a,b], **David S. Ruch**[a], **Farshid Guilak**[a,b], and **Dianne Little**[a,*]

[a]Department of Orthopaedic Surgery, Duke University Medical Center, Durham, NC 27710, USA

[b]Department of Biomedical Engineering, Duke University, Durham, NC 27708, USA

Abstract

The rotator cuff consists of several tendons and muscles that provide stability and force transmission in the shoulder joint. Whereas most rotator cuff tears are amenable to suture repair, the overall success rate of repair is low, and massive tears are prone to re-tear. Extracellular matrix (ECM) patches are used to augment suture repair, but they have limitations. Tissue-engineered approaches provide a promising solution for massive rotator cuff tears. Previous studies have shown that, compared to nonaligned scaffolds, aligned electrospun polymer scaffolds exhibit greater anisotropy and exert a greater tenogenic effect. Nevertheless, achieving rapid cell infiltration through the full thickness of the scaffold is challenging, and scaling to a translationally relevant size may be difficult. Our goal was to evaluate whether a novel method of alignment, combining a multilayered electrospinning technique with a hybrid of several electrospinning alignment techniques, would permit cell infiltration and collagen deposition through the thickness of poly(ε-caprolactone) scaffolds following seeding with human adipose-derived stem cells. Furthermore, we evaluated whether multilayered aligned scaffolds enhanced collagen alignment, tendon-related gene expression, and mechanical properties compared to multilayered nonaligned scaffolds. Both aligned and nonaligned multilayered scaffolds demonstrated cell infiltration and ECM deposition through the full thickness of the scaffold after only 28 days of culture. Aligned scaffolds displayed significantly increased expression of tenomodulin compared to nonaligned scaffolds and exhibited aligned collagen fibrils throughout the full thickness, the presence of which may account for the increased yield stress and Young's modulus of cell-seeded aligned scaffolds along the axis of fiber alignment.

Graphical abstract

*Address correspondence to: Dr. Dianne Little, Orthopaedic Research Laboratories, DUMC Box 3093, 375 MSRB1, Durham, NC 27710, USA. Tel.: (919) 681-6867; fax: (919) 681-8490. dianne.little@duke.edu.

Disclosures

D.S.R. is a paid consultant for Acumed. F.G. is a paid employee of and holds stock in Cytex Therapeutics. D.L. is a paid consultant for Cytex Therapeutics.

Data from this study were presented as a poster at the 2014 annual meeting of the Orthopedic Research Society.

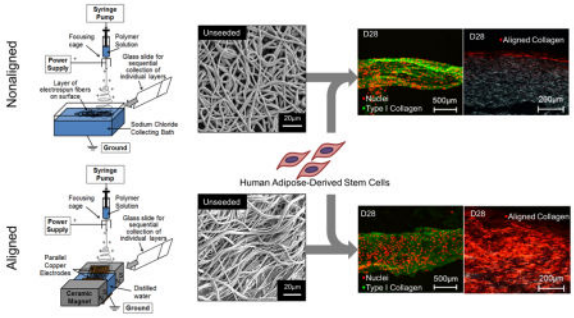

Keywords

Electrospinning; Adipose-derived stem cell; Nanofiber; Microfiber; Tissue engineering

1. Introduction

The prevalence of rotator cuff tears increases with age to >50% in individuals over the age of 60 [1,2]. Currently, over 300,000 surgeries are performed annually in the United States to repair rotator cuff tears [3], and this number is likely to rise with the projected increase in elderly populations [4]. Re-tear rates are high, especially with increasing tear size [5,6], and massive rotator cuff tears may not be amenable to traditional suture repair [7]. In this regard, tissue engineering approaches to enhance or augment traditional suture rotator cuff repair could have significant clinical impact. Extracellular matrix (ECM) patches have been used to augment repair but generally have inadequate mechanical properties [8], and slow cell infiltration prevents rapid integration of many commercially available ECM patches [9,10].

Therefore, there is a need for tissue-engineered approaches that both stimulate rapid tendon healing and provide adequate mechanical augmentation for the rotator cuff [11]. Electrospun scaffolds have shown significant potential in this regard [12–15], but do not yet provide adequate mechanical properties. A further challenge has been achieving cell infiltration through the full thickness of the scaffold [16,17]. Various methods to improve porosity of the electrospun scaffold have been evaluated [16,18–22]. To address this need specifically for rotator cuff tendon tissue engineering, we have recently modified a multilayered electrospinning technique [22] to achieve rapid infiltration of human adipose-derived stem cell (hASC) and tenogenic ECM synthesis through the full thickness of randomly multilayered electrospun scaffolds [23]. However, several recent studies indicate that, compared with nonaligned or randomly oriented fibers, aligned nanofibers can enhance tenogenesis [12,24,25]. Furthermore, such fiber alignment creates mechanical anisotropy that more closely mimics tendon mechanical properties. Electrospun fiber alignment can be achieved through the use of a rotating disc [26–28], rotating mandrel [29–31], patterned electrodes [32,33], air-gap techniques [34,35], patterned insulators [36], or ceramic magnets [37–39]. However, as with nonaligned scaffolds, achieving cell infiltration can be problematic when using rotating mandrel techniques, unless sacrificial fibers are simultaneously co-spun [16,40]. Air-gap techniques are typically limited by short lengths of fiber alignment (~1 cm) [41] or by decreasing alignment with increasing duration of electrospinning [35]. Multilayered aligned scaffolds (produced by stacking aligned layers on

top of each other) across short lengths of fiber alignment have previously been reported to control the hierarchical structure within the scaffold [36,42], and thus may be advantageous for the development of scaffolds for rotator cuff tendon tissue engineering [24,25]. The objectives of this study were to (1) to develop a novel multilayered electrospinning technique that allows for prescribed alignment of each layer in a clinically relevant patch size, and (2) to evaluate the ability of these aligned scaffolds to induce complete cellular infiltration, tenogenic ECM formation, and development of tensile mechanical properties by hASCs compared to nonaligned multilayered scaffolds.

2. Materials and methods

2.1. Aligned multilayered electrospun scaffolds

Poly(ε-caprolactone) (PCL) (Mn = 80,000) (Sigma-Aldrich, St. Louis, MO) was dissolved at 100 mg/mL in 7:3 dichloromethane:ethanol for 24 h before use. Individual alignment methods (ceramic magnets, air-gap, patterned insulators, parallel copper electrodes) amenable to formation of multilayered square or rectangular patch scaffolds were first screened for their ability to induce aligned fiber formation over air-gaps of 5–8 cm, a size relevant for future clinical use. Each method of alignment was screened systematically using a range of polymer flow rates, voltages, needle sizes, needle-ground distance, and spinning times to most closely match fibers obtained using nonaligned techniques (see Section 2.2). As has been previously reported [32–34, 36–39], each individual method was able to induce fiber alignment over a short (1–3 cm) air-gap, but as the size of the air-gap was increased, alignment was lost or was evident for progressively shorter periods of time before deposition of fibers occurred elsewhere (Fig. S1). However, when individual alignment methods were combined to include ceramic magnets and parallel copper electrodes outside of a rectangular rubber-coated reservoir containing distilled water (volume dependent on ambient temperature and humidity), robust aligned layers were obtained for up to 5 min of electrospinning across an air-gap of 10 cm. Therefore, the final electrospinning apparatus used (Fig. 1) was a rectangular, rubber-coated reservoir (10 cm wide × 15 cm long) containing distilled water, with grounded 6-cm wide parallel copper electrodes immediately outside of the reservoir centered at the midpoint of the reservoir length and immediately surrounded by ceramic magnets (2.5 cm × 7 cm × 14.5 cm) oriented to attract each other. The following electrospinning parameters were used: 21 G needle fitted with a round wire mesh focusing cage (3 cm diameter, needle tip protruding 4 mm from bottom of cage), 5 mL/h, 16 kV, and a 13.5 cm needle-to-ground distance. Aligned layers were collected sequentially from the surface of the saline bath every 3 min onto a 5 cm × 7.5 cm glass slide, for a total of 140 layers (approximately 1 mm thick).

2.2. Nonaligned multilayered scaffolds

Nonaligned multilayered scaffolds were prepared by electrospinning into a grounded saline bath (1.25 g/L NaCl in distilled water) using the apparatus previously described (Fig. 1) [23]. PCL was electrospun using the following parameters: 25 G needle fitted with a round wire mesh focusing cage (3 cm diameter, needle tip protruding 4 mm from bottom of cage), 2.5 mL/h, 17 kV, and a 17 cm needle-to-ground distance. Nonaligned layers were collected sequentially from the surface of the saline bath every 2 min using a 5 cm × 7.5 cm glass

slide, for a total of 70 layers (approximately 1 mm thick). Parameters were selected to obtain similar scaffold thickness and fiber diameters between aligned and nonaligned scaffolds (Section 3). For all scaffolds produced, relative humidity was 20%–40%, and ambient temperature ranged from 18 °C to 25 °C. Each scaffold was allowed to dry at room temperature and then stored at room temperature protected from light until use.

2.3. Fiber diameter analysis

Three 0.5 cm × 1 cm strips were cut from each scaffold (center and two orthogonal edges), sterilized (see Section 2.4), critical point dried in CO_2, and then sputter coated with gold. Each sample was viewed with a Philips 501 scanning electron microscope. Three representative images were taken of each sample, and diameter of 100–150 fibers for each type of scaffold was measured in ImageJ (NIH, USA).

2.4. Cell seeding and culture

Scaffolds were cut into individual 0.5 cm × 1 cm strips with long axis parallel to the expected direction of fiber alignment and sutured to a Teflon ring to maintain shape and suspension in media. Scaffolds to be used for mechanical testing were cut into dog-bone shapes in directions parallel and perpendicular to the direction of expected alignment, and similarly for nonaligned scaffolds. Each scaffold was rehydrated and sterilized in a graded series of ethanol baths to improve seeding before a final 30-min rinse in phosphate-buffered saline (PBS) at pH 7.4. Both sides of each scaffold were sterilized under ultraviolet light for 10 min and pre-wetted with PBS before cell seeding. We isolated hASCs by collagenase digestion of lipoaspirate surgical waste from five de-identified female donors (age 36–59, body mass index 19.6–33.1) with approval of the Duke University Institutional Review Board and used the cells at passage 4 [23,43]. Cells were seeded at a density of 1×10^6 hASCs/cm^2 for quantitative real-time reverse transcription polymerase chain reaction (qRT-PCR) and 0 or 0.5×10^6 hASCs/cm^2 for all other assays. Half of the cells were seeded onto one side of the scaffold by direct pipetting and allowed to attach for 15 min, before the scaffolds were turned over and the procedure repeated. No gross differences in wettability or in cell seeding were noted between aligned and nonaligned scaffolds. Scaffolds were then maintained in 6-well plates coated with 2% agarose without growth factors at 37 °C and 5% CO_2 in Advanced DMEM (Life Technologies) supplemented with 10% fetal bovine serum (Zen-Bio), 1% penicillin–streptomycin–fungizone (Life Technologies), 4 mM L-glutamine (Life Technologies), and 15 mM l-ascorbic acid-2-phosphate (Sigma-Aldrich), which was changed every other day for the designated culture periods.

2.5. Biochemical assays

On days 0, 7, 14, and 28, unseeded and hASC-seeded nonaligned and aligned scaffolds (n=5 per group) were harvested and lyophilized to obtain dry weight. Samples were pulverized and digested for 1 week in papain (125 μg/mL) at 60 °C. The dsDNA content was quantified using the Picogreen Assay (Life Technologies). The sulfated glycosaminoglycan (s-GAG) content was quantified spectrophotometrically using the 1,9-dimethylmethylene blue dye (pH 3.0) [44]. The hydroxyproline assay was used to determine the total collagen content

using a conversion factor of 1:7.46 to convert hydroxyproline to collagen [45]. All results were normalized to dry weight (mean ± SD).

2.6. RNA isolation and real-time qRT-PCR

RNA was extracted from hASC-seeded aligned and nonaligned scaffolds (n=5 per group) pulverized after harvest at 4, 7, and 14 days of cell culture, and from a pellet of cells of the same passage not seeded onto scaffolds, using the QiaShredder column (Qiagen) followed by the RNeasy Mini kit (Qiagen). Equal amounts of RNA were reverse transcribed using the Superscript VILO cDNA Synthesis Kit (Life Technologies). Real-time qRT-PCR was performed on a StepOnePlus (Applied Biosystems) using Express qPCR SuperMix (Invitrogen) as described previously for glyceraldehyde-3-phosphate dehydrogenase (*GAPDH*, endogenous control, assay ID Hs02758991_g1) and six tendon-related genes: type I collagen (*COL1A1*), type III collagen (*COL3A1*), decorin (*DCN*), biglycan (*BGN*), tenomodulin (*TNMD*), and tenascin C (*TNC*) [23]. Data from each gene of interest for each sample were corrected for efficiency and normalized to expression of *GAPDH*. These data were then expressed as fold-change relative to the level of gene expression in 1 million P4 hASCs before cell seeding from each donor at day 0 [46].

2.7. Histology

Unseeded and hASC-seeded aligned and unaligned scaffolds (n=5) were harvested after 28 days of culture, embedded in optimal cutting temperature gel (Sakura), and frozen at −80 °C. We mounted 10-μm sections on slides and evaluated them under a Zeiss LSM 510 Confocal Microscope (Carl Zeiss) after immunofluorescence labeling of human type I and III collagen, as described previously [43].

2.8. Analysis of scaffold and matrix alignment

Evaluation of scaffold and ECM alignment was performed in two ways: First, 10 μm sections were digested with hyaluronidase after 0 and 28 days of culture (n=5 per group) and stained with 0.1% Picrosirius Red solution for analysis of aligned fibrillar collagen relative to the vertical gradient through the thickness of the scaffold using polarized light microscopy [47]. Second, aligned and unaligned scaffolds were harvested after 0, 7, and 28 days of culture (n=5 per group), fixed in 2.5% glutaraldehyde, incubated in osmium tetroxide, washed in PBS, dehydrated in a graded series of ethanol washes, and incubated in tetramethylsilane. After desiccation, samples were sputter coated and imaged by scanning electron microscope as described above. Six images were taken of each sample, then fast Fourier transform (FFT) was performed using a custom MATLAB (MathWorks, Natick, MA) code [36], based on a modification of a previously described method [30]. FFTs from each image of the same scaffold type and time point were averaged and normalized to show the actual angle of alignment relative to the expected angle of alignment. The fiber alignment index was calculated from the average magnitude of the FFT profile for 15° on each side of the expected orientation [36].

2.9. Mechanical testing

After harvest at day 0 or 28, hASC-seeded dog-bone samples oriented parallel and perpendicular to the expected axis of alignment (n=6 per group) were wrapped in gauze soaked in PBS and stored at −80 °C until analysis. Samples were marked at 5-mm increments from the center of the dog bone to allow regional strain analysis, and initial scaffold thickness was measured using a digital camera (Allied Vision Technologies, Inc.) and digital calipers in ImageJ. Samples were tested as previously described [23], in tension at a strain rate of 1%/s with 0.5 g preload using an electromechanical testing system (Bose Enduratec Smart Test Series; Bose Corporation) with a 2.27 kg load cell (Sensotec Model 31; Honeywell International). Mid-substance strains were calculated from digital images acquired at 20 Hz and interpolated to load frame data using custom MATLAB code [23]. The Young's modulus of the linear region and stretch and stress at yield were calculated in Microsoft Excel.

2.10. Statistical analysis

Data are reported as median and interquartile range (25^{th}–75^{th} percentile) or mean ± SD, tested for normality, transformed using Box-Cox transformation if necessary, and then evaluated for the effect of scaffold alignment, seeding, and time using factorial analysis of variance (ANOVA). The Newman–Keuls *post hoc* test was used to determine differences between treatments following ANOVA. Significance was reported at the 95% confidence level for all analyses (α=0.05).

3. Results

Median fiber diameter of nonaligned scaffolds was 1.57 μm (1.20–2.53), and not significantly different (p=0.61) than those of aligned scaffolds, 1.76 μm (1.06–2.58). Scaffold thickness was reduced and different between scaffolds at the time of use relative to the thickness immediately after electrospinning (approximately 1 mm thick); aligned scaffolds were 0.43 ± 0.18 mm thick and nonaligned were 0.75 ± 0.132 mm thick (p<0.001). dsDNA, s-GAG, and collagen content of all scaffolds increased after cell seeding, and there was no effect of fiber alignment (Fig. 2). On both types of scaffolds, gene expression was consistent with tenogenesis (Fig. 3). Between scaffold types, *COL3A1* and *TNMD* expression was increased on aligned relative to nonaligned scaffolds (Fig. 3). Both aligned and nonaligned scaffolds demonstrated cell infiltration through the full thickness of the scaffold and type I and III collagen synthesis through the full thickness of the scaffold (Fig. 4). However, total collagen through the full thickness of the scaffolds, as assessed by Picrosirius Red, was more abundant in aligned scaffolds. Under polarized light microscopy, only aligned scaffolds demonstrated substantial red birefringence through the full thickness of the scaffold (Fig. 4). This electrospinning alignment technique produced scaffolds with a fiber alignment index approximately 17 times greater than nonaligned scaffolds (Fig. 5), and was oriented in the expected direction of alignment. Fiber alignment index remained significantly greater in aligned scaffolds compared to nonaligned after 7 days of culture. However, by 28 days of culture, the fiber alignment index on the surface of aligned scaffolds was significantly less than nonaligned scaffolds at the same time point and less than aligned scaffolds at Day 0 and 7 (Fig. 5). Nonaligned scaffolds demonstrated an increase in fiber

alignment index in the first 7 days of culture, and a small but significant decrease in fiber alignment index by 28 days of culture (Fig. 5). Aligned scaffolds showed significant anisotropy with respect to Young's modulus and yield stress, whereas unaligned scaffolds were isotropic (Fig. 6). After 28 days of culture, aligned scaffolds demonstrated significantly increased modulus and yield stress along the axis of fiber alignment, as compared to all other groups tested. Nonaligned scaffolds demonstrated an increase in Young's modulus over time, but no significant increase in yield stress or yield stretch with culture. Yield stretch (Fig. 6) did not demonstrate anisotropy but increased with cell seeding, and was greatest in aligned scaffolds.

4. Discussion

The novel multilayered alignment technique evaluated in this study demonstrated enhanced tensile mechanical properties and development of fibrillar collagen though the full thickness of a clinically relevant sized-scaffold after 28 days of culture compared to nonaligned multilayered scaffolds. These findings were accompanied by increases in *TNMD* and *COL3A1* expression, and at early post-seeding time points, alignment of newly synthesized ECM on the surface of the scaffolds. Additionally, in both aligned and nonaligned scaffolds, we found complete cellular infiltration and type I and III collagen synthesis through the full thickness of the scaffolds, and gene expression consistent with tenogenesis and with our previous findings [23].

The most commonly reported technique for alignment of electrospun fibers is the use of a rotating ground electrode (i.e., mandrel or disc) [26–31,48]. While this technique readily allows for collection of a patch-like scaffold, achieving cell infiltration through scaffolds prepared in this manner requires the use of sacrificial fibers [16], a combination of electrospinning and electrospraying [16,40,49], or incorporation of biomimetic materials into the scaffold [50]. The alignment method used in this study was a hybrid of several other techniques previously reported, and it further improved cellular infiltration and control of fiber alignment over clinically relevant scales as compared to these techniques used individually. Using the combination of alignment methods described, we achieved fiber alignment over an air-gap of 10 cm and successfully maintained fiber alignment with increasing fiber deposition for electrospinning periods of up to 10 min as has been reported with another similar technique [35].

As previously reported on nonaligned multilayered scaffolds [23], dsDNA, s-GAG, and collagen content increased over time in culture, but in this study there was no additional beneficial effect of scaffold alignment on the amount of matrix production. This phenomenon is consistent with previous studies, as matrix production in response to fiber alignment appears to be dependent primarily on cell type. For example, bone marrow derived mesenchymal stem cells (MSCs) but not rotator cuff tendon fibroblasts demonstrate increased proliferation and collagen synthesis on aligned nanofibers compared to nonaligned nanofibers on scaffolds of equivalent fiber diameter and cultured at similar density and in similar media [12,51]. Furthermore, anterior cruciate ligament fibroblasts increased proliferation and collagen synthesis on aligned scaffolds compared to nonaligned, although fiber diameter of nonaligned scaffolds was not described [52]. Others have shown that

whereas bovine MSCs produce more ECM on aligned nanofibrous scaffolds than in pellet culture compared to donor-matched meniscal fibrochondrocytes, the opposite effect is observed in human MSCs [53,54].

The overall gene expression patterns observed in this study are consistent with tenogenesis and with our previous results in hASCs [23,43]. In particular, the increase in *DCN* and initial decrease in *BGN* expression are consistent with tendon regeneration rather than repair [55,56]. *TNMD* is necessary for tenocyte proliferation and collagen fibril maturation [57]; thus, the differential upregulation of *TNMD* on aligned scaffolds in this study is consistent with the finding of increased fibrillar collagen through the full thickness of aligned but not unaligned scaffolds, but investigation of other ECM components such as type VI collagen would be required to definitively link these findings [57]. Other studies evaluating gene expression on aligned and nonaligned scaffolds have not found differences in tendon gene expression between aligned and nonaligned nanofibers [12,51,58]. However, in this study, fiber diameter was more than double that reported in others [12,51], and micro- rather than nanofiber diameter has been found to promote expression of tendon phenotypic markers by human fibroblasts, notably *COL1A1*, *COL3A1*, and *TNMD* [59].

In this study, robust cell infiltration and type I and III collagen synthesis were observed through the full thickness of the scaffold after only 28 days in culture as we have seen previously for nonaligned scaffolds [23], irrespective of fiber alignment. This finding is in contrast to other *in vitro* studies, in which complete cell infiltration required 70 days of culture in aligned scaffolds [53], unless sacrificial fibers were included within the scaffold to achieve complete cell infiltration within 21 days [16]. The rate of cellular infiltration occurred was not specifically evaluated in this study, but in the original description of the nonaligned multilayered technique used here, Tzezana et al. [22] found almost complete infiltration of myofibroblasts or embryonic stem cells by 14 days after seeding compared to single-layer scaffolds, and suggested that enhanced cellular migration in multilayered scaffolds may be facilitated through enhanced interconnectivity between individual pores. In support of this, we have previously found infiltration of cells through only the outer third of nonaligned single-layer scaffolds after 28 days of culture, in contrast to full-thickness infiltration in nonaligned 60-layer scaffolds at the same time point [36]. Despite similar type I and III collagen synthesis identified by immunofluorescence microscopy between aligned and nonaligned scaffolds, and similar collagen synthesis assessed by hydroxyproline assay, Picrosirius Red staining was enhanced on aligned compared to nonaligned scaffolds, and when evaluated by polarized light microscopy, red birefringence was present through the full thickness of the scaffolds in aligned but not nonaligned scaffolds. This finding indicates that the interior of aligned multilayered electrospun scaffolds supports development of both larger diameter and more aligned collagen fibrils compared to nonaligned multilayered scaffolds [60].

Examination of the surface alignment of the newly deposited ECM and cells demonstrated the expected alignment with aligned fiber orientation at 7 but not 28 days of culture. This finding is in contrast to another study in which cell alignment persisted on the surface of aligned scaffolds after 28 days [51]. However, initial cell seeding density in that study was 10-fold lower than the current study, and cells were not confluent on the surface of the

scaffolds after 28 days of culture. Emerging evidence suggests that response to microarchitectural cues, cell proliferation, migration, symmetry of cell-cell contacts, and direction of cellular and matrix alignment are tightly coordinated [61–65]. In the initial period after seeding on electrospun fibers, MSCs demonstrate potent directionality in their migration response and in their cell-cell contacts on aligned compared to nonaligned electrospun fibers [66]. In contrast, once cells are confluent on the surface of electrospun scaffolds and lose contact with fibers, cell-cell contact may become the predominant driver of direction of cellular alignment, unless mechanical stimulation is applied to the scaffolds to maintain alignment [51,67,68]. This loss of cell interaction with aligned fibers that occurs at the surface, leading to loss of overall cell alignment, does not occur in the three-dimensional fiber environment of the interior of the scaffold where cells continue to stimulate development of aligned collagen in aligned but not nonaligned scaffolds. In nonaligned multilayered scaffolds after seeding, surface cellular and matrix organization was not randomly oriented, since there were regions of local alignment within each nonaligned scaffold, similar to that reported previously (Fig. 5A) [36]. Interestingly, and in contrast to our previous study, there was a small but significant increase in fiber alignment index after 7 days on seeded nonaligned scaffolds compared to unseeded nonaligned scaffolds, in the direction of the long axis of the 0.5 cm × 1 cm cultured scaffold. This may be due to domination of macro-scale edge or boundary effects over the nano- and micro-scale architecture resulting in asymmetric cell-cell contacts and is the subject of current studies [61–63, 65]. The surface alignment of cells and matrix on nonaligned scaffolds at day 7 was attenuated by 28 days, suggesting that boundary conditions may not be sufficient to maintain alignment on nonaligned scaffolds once cells become super-confluent on the surface, and that mechanical load may be necessary to maintain and increase alignment [51].

The rapid synthesis of aligned fibrillar collagen in aligned scaffolds may account for the rapid increase in Young's modulus and yield stress of aligned hASC-seeded scaffolds after only 28 days in culture, and for the maintenance of anisotropy even in the absence of mechanical loading. The Young's modulus of these scaffolds after 28 days of culture is still only approximately 20–25% of that of the human supraspinatus tendon [69,70], but is of the same order of magnitude as many of the currently available ECM patches [71]. PCL, chosen for its neutral degradation profile and relatively slow degradation rate [72], has a relatively low tensile modulus when compared to many polymers commonly used in electrospinning for tissue engineering [73]. Continued evaluation of this technique using alternative polymers is likely to improve on these mechanical properties. One advantage of this multilayered alignment technique is that we can readily manipulate the alignment of individual layers within the vertical gradient and over different regions of the scaffold. This may ultimately reduce mismatch and stress concentration between the scaffold and the underlying supraspinatus tendon [74]. Additionally, since mechanical loading augments the effects of fiber alignment, further improvement in tensile mechanical properties are expected in bioreactor and *in vivo* studies.

5. Conclusions

In summary, the novel multilayered alignment technique described here produced anisotropic scaffolds up to 7.5 cm × 10 cm of a clinically relevant size and thickness that

permitted early and complete cellular infiltration through the full thickness of the scaffold by hASCs, enhanced *TNMD* and *COL3A1* expression, alignment of newly synthesized fibrillar collagen, and early development of tensile mechanical properties compared to multilayered nonaligned scaffolds. With continued evaluation, this technique should lead to development of a new augmentation patch to improve on currently available treatment options for rotator cuff tear repair.

Supplementary Material

Refer to Web version on PubMed Central for supplementary material.

Acknowledgments

This study was supported in part by National Institutes of Health grants AR59784 (to D.L.), AR065764 (to D.L.), AR48852 (to F.G.), AG15768 (to F.G.), AR48182 (to F.G.), AR50245 (to F.G.), AG46927 (to F.G.), and AR65888 (to C.L.G) and by Synthes USA.

References

1. Sher JS, Uribe JW, Posada A, Murphy BJ, Zlatkin MB. Abnormal findings on magnetic resonance images of asymptomatic shoulders. J Bone Joint Surg Am. 1995; 77:10–5. [PubMed: 7822341]
2. Yamaguchi K, Ditsios K, Middleton WD, Hildebolt CF, Galatz LM, Teefey SA. The demographic and morphological features of rotator cuff disease: a comparison of asymptomatic and symptomatic shoulders. J Bone Joint Surg Am. 2006; 88:1699–704. [PubMed: 16882890]
3. Colvin AC, Egorova N, Harrison AK, Moskowitz A, Flatow EL. National trends in rotator cuff repair. J Bone Joint Surg Am. 2012; 94:227–33. [PubMed: 22298054]
4. De Carvalho BR, Puri A, Calder JA. Open rotator cuff repairs in patients 70 years and older. ANZ Journal of Surgery. 2012; 82:461–5. [PubMed: 22519638]
5. Wu XL, Briggs L, Murrell GA. Intraoperative determinants of rotator cuff repair integrity: an analysis of 500 consecutive repairs. Am J Sports Med. 2012; 40:2771–6. [PubMed: 23104609]
6. Galatz LM, Ball CM, Teefey SA, Middleton WD, Yamaguchi K. The outcome and repair integrity of completely arthroscopically repaired large and massive rotator cuff tears. J Bone Joint Surg Am. 2004; 86-A:219–24. [PubMed: 14960664]
7. Matthews TJW, Hand GC, Rees JL, Athanasou NA, Carr AJ. Pathology of the torn rotator cuff tendon: reduction in potential for repair as tear size increases. J Bone Joint Surg Br. 2006; 88-B: 489–95. [PubMed: 16567784]
8. Derwin KA, Baker AR, Spragg RK, Leigh DR, Iannotti JP. Commercial extracellular matrix scaffolds for rotator cuff tendon repair: biomechanical, biochemical, and cellular properties. J Bone Joint Surg Am. 2006; 88:2665–72. [PubMed: 17142417]
9. Cornwell KG, Landsman A, James KS. Extracellular matrix biomaterials for soft tissue repair. Clin Podiatr Med Surg. 2009; 26:507–23. [PubMed: 19778685]
10. Shea KP, McCarthy MB, Ledgard F, Arciero C, Chowaniec D, Mazzocca AD. Human tendon cell response to 7 commercially available extracellular matrix materials: an in vitro study. Arthroscopy. 2010; 26:1181–8. [PubMed: 20630692]
11. Iannotti JP, Deutsch A, Green A, Rudicel S, Christensen J, Marraffino S, Rodeo S. Time to failure after rotator cuff repair: a prospective imaging study. J Bone Joint Surg Am. 2013; 95:965–71. [PubMed: 23780533]
12. Moffat KL, Kwei AS, Spalazzi JP, Doty SB, Levine WN, Lu HH. Novel nanofiber-based scaffold for rotator cuff repair and augmentation. Tissue Eng Part A. 2009; 15:115–26. [PubMed: 18788982]
13. Inui A, et al. Regeneration of rotator cuff tear using electrospun poly(d,l-Lactide-Co-Glycolide) scaffolds in a rabbit model. Arthroscopy. 2012; 28:1790–9. [PubMed: 23058811]

14. Hakimi O, Murphy R, Stachewicz U, Hislop S, Carr AJ. An electrospun polydioxanone patch for the localisation of biological therapies during tendon repair. Eur Cell Mater. 2012; 24:344–57. [PubMed: 23090765]
15. Beason DP, Connizzo BK, Dourte LM, Mauck RL, Soslowsky LJ, Steinberg DR, Bernstein J. Fiber-aligned polymer scaffolds for rotator cuff repair in a rat model. J Shoulder Elbow Surg. 2012; 21:245–50. [PubMed: 22244068]
16. Baker BM, Gee AO, Metter RB, Nathan AS, Marklein RA, Burdick JA, Mauck RL. The potential to improve cell infiltration in composite fiber-aligned electrospun scaffolds by the selective removal of sacrificial fibers. Biomaterials. 2008; 29:2348–58. [PubMed: 18313138]
17. Zhong S, Zhang Y, Lim CT. Fabrication of large pores in electrospun nanofibrous scaffolds for cellular infiltration: a review. Tissue Eng Part B Rev. 2012; 18:77–87. [PubMed: 21902623]
18. Baker BM, Shah RP, Silverstein AM, Esterhai JL, Burdick JA, Mauck RL. Sacrificial nanofibrous composites provide instruction without impediment and enable functional tissue formation. Proc Natl Acad Sci USA. 2012; 109:14176–81. [PubMed: 22872864]
19. Levorson EJ, Sreerekha PR, Chennazhi KP, Kasper FK, Nair SV, Mikos AG. Fabrication and characterization of multiscale electrospun scaffolds for cartilage regeneration. Biomed Mater. 2013; 8:014103. [PubMed: 23353096]
20. McCullen SD, Miller PR, Gittard SD, Gorga RE, Pourdeyhimi B, Narayan RJ, Loboa EG. In situ collagen polymerization of layered cell-seeded electrospun scaffolds for bone tissue engineering applications. Tissue Eng Part C Methods. 2010; 16:1095–105. [PubMed: 20192901]
21. Nam J, Huang Y, Agarwal S, Lannutti J. Improved cellular infiltration in electrospun fiber via engineered porosity. Tissue Eng. 2007; 13:2249–57. [PubMed: 17536926]
22. Tzezana R, Zussman E, Levenberg S. A layered ultra-porous scaffold for tissue engineering, created via a hydrospinning method. Tissue Eng Part C Methods. 2008; 14:281–8. [PubMed: 18781888]
23. Chainani A, Hippensteel KJ, Kishan A, Garrigues NW, Ruch DS, Guilak F, Little D. Multilayered electrospun scaffolds for tendon tissue engineering. Tissue Eng Part A. 2013; 19:2594–604. [PubMed: 23808760]
24. Shang S, Yang F, Cheng X, Walboomers XF, Jansen JA. The effect of electrospun fibre alignment on the behaviour of rat periodontal ligament cells. Eur Cell Mater. 2010; 19:180–92. [PubMed: 20419630]
25. Yin Z, Chen X, Chen JL, Shen WL, Hieu Nguyen TM, Gao L, Ouyang HW. The regulation of tendon stem cell differentiation by the alignment of nanofibers. Biomaterials. 2010; 31:2163–75. [PubMed: 19995669]
26. Salalha W, Dror Y, Khalfin RL, Cohen Y, Yarin AL, Zussman E. Single-walled carbon nanotubes embedded in oriented polymeric nanofibers by electrospinning. Langmuir. 2004; 20:9852–5. [PubMed: 15491224]
27. Yang F, Murugan R, Wang S, Ramakrishna S. Electrospinning of nano/micro scale poly(L-lactic acid) aligned fibers and their potential in neural tissue engineering. Biomaterials. 2005; 26:2603–10. [PubMed: 15585263]
28. Theron A, Zussman E, Yarin AL. Electrostatic field-assisted alignment of electrospun nanofibres. Nanotechnology. 2001; 12:384–90.
29. Baker SC, Atkin N, Gunning PA, Granville N, Wilson K, Wilson D, Southgate J. Characterisation of electrospun polystyrene scaffolds for three-dimensional in vitro biological studies. Biomaterials. 2006; 27:3136–46. [PubMed: 16473404]
30. Ayres C, et al. Modulation of anisotropy in electrospun tissue-engineering scaffolds: analysis of fiber alignment by the fast Fourier transform. Biomaterials. 2006; 27:5524–34. [PubMed: 16859744]
31. Li WJ, Mauck RL, Cooper JA, Yuan X, Tuan RS. Engineering controllable anisotropy in electrospun biodegradable nanofibrous scaffolds for musculoskeletal tissue engineering. J Biomech. 2007; 40:1686–93. [PubMed: 17056048]
32. Li D, Ouyang G, McCann JT, Xia Y. Collecting electrospun nanofibers with patterned electrodes. Nano Lett. 2005; 5:913–6. [PubMed: 15884893]

33. Zhou W, Li Z, Zhang Q, Liu Y, Wei F, Luo G. Gas flow-assisted alignment of super long electrospun nanofibers. J Nanosci Nanotechnol. 2007; 7:2667–73. [PubMed: 17685282]
34. Lim JM, Moon JH, Yi GR, Heo CJ, Yang SM. Fabrication of one-dimensional colloidal assemblies from electrospun nanofibers. Langmuir. 2006; 22:3445–9. [PubMed: 16584206]
35. Sell SA, McClure MJ, Ayres CE, Simpson DG, Bowlin GL. Preliminary investigation of airgap electrospun silk-fibroin-based structures for ligament analogue engineering. J Biomater Sci Polym Ed. 2010 Epub ahead of print.
36. Garrigues NW, Little D, O'Conor CJ, Guilak F. Use of an insulating mask for controlling anisotropy in multilayer electrospun scaffolds for tissue engineering. J Mater Chem. 2010; 20:8962–8. [PubMed: 21072247]
37. Yang D, Lu B, Zhao Y, Jiang X. Fabrication of aligned fibrous arrays by magnetic electrospinning. Adv Mat. 2007; 19:3702–6.
38. Liu Y, Zhang X, Xia Y, Yang H. Magnetic-field assisted electrospinning of aligned straight and wavy polymeric nanofibers. Adv Mat. 2010; 22:2454–7.
39. Yang D, Zhang J, Ahang J, Nie J. Aligned electrospun nanofibers induced by magnetic field. J Appl Polym Sci. 2008; 110:3368–72.
40. Hashizume R, et al. Morphological and mechanical characteristics of the reconstructed rat abdominal wall following use of a wet electrospun biodegradable polyurethane elastomer scaffold. Biomaterials. 2010; 31:3253–65. [PubMed: 20138661]
41. Chaurey V, Chiang PC, Polanco C, Su YH, Chou CF, Swami NS. Interplay of electrical forces for alignment of sub-100 nm electrospun nanofibers on insulator gap collectors. Langmuir. 2010; 26:19022–6. [PubMed: 21082824]
42. Li D, Wang Y, Xia Y. Electrospinning nanofibers as uniaxially aligned arrays and layer-by-layer stacked films. Adv Mat. 2004; 16:361–6.
43. Little D, Guilak F, Ruch DS. Ligament-derived matrix stimulates a ligamentous phenotype in human adipose-derived stem cells. Tissue Eng Part A. 2010; 16:2307–19. [PubMed: 20406104]
44. Enobakhare BO, Bader DL, Lee DA. Quantification of sulfated glycosaminoglycans in chondrocyte/alginate cultures, by use of 1,9-dimethylmethylene blue. Anal Biochem. 1996; 243:189–91. [PubMed: 8954546]
45. Neidert MR, Lee ES, Oegema TR, Tranquillo RT. Enhanced fibrin remodeling in vitro with TGF-beta1, insulin and plasmin for improved tissue-equivalents. Biomaterials. 2002; 23:3717–31. [PubMed: 12109697]
46. Pfaffl MW. A new mathematical model for relative quantification in real-time RT-PCR. Nucleic Acids Res. 2001; 29:e45. [PubMed: 11328886]
47. Thomopoulos S, Marquez JP, Weinberger B, Birman V, Genin GM. Collagen fiber orientation at the tendon to bone insertion and its influence on stress concentrations. J Biomech. 2006; 39:1842–51. [PubMed: 16024026]
48. Mauck RL, Baker BM, Nerurkar NL, Burdick JA, Li WJ, Tuan RS, Elliott DM. Engineering on the straight and narrow: the mechanics of nanofibrous assemblies for fiber-reinforced tissue regeneration. Tissue Eng Part B Rev. 2009; 15:171–93. [PubMed: 19207040]
49. Stankus JJ, Guan J, Fujimoto K, Wagner WR. Microintegrating smooth muscle cells into a biodegradable, elastomeric fiber matrix. Biomaterials. 2006; 27:735–44. [PubMed: 16095685]
50. Stankus JJ, Freytes DO, Badylak SF, Wagner WR. Hybrid nanofibrous scaffolds from electrospinning of a synthetic biodegradable elastomer and urinary bladder matrix. J Biomater Sci Polym Ed. 2008; 19:635–52. [PubMed: 18419942]
51. Subramony SD, Dargis BR, Castillo M, Azeloglu EU, Tracey MS, Su A, Lu HH. The guidance of stem cell differentiation by substrate alignment and mechanical stimulation. Biomaterials. 2013; 34:1942–53. [PubMed: 23245926]
52. Lee CH, Shin HJ, Cho IH, Kang YM, Kim IA, Park KD, Shin JW. Nanofiber alignment and direction of mechanical strain affect the ECM production of human ACL fibroblast. Biomaterials. 2005; 26:1261–70. [PubMed: 15475056]
53. Baker BM, Mauck RL. The effect of nanofiber alignment on the maturation of engineered meniscus constructs. Biomaterials. 2007; 28:1967–77. [PubMed: 17250888]

54. Baker BM, Nathan AS, Gee AO, Mauck RL. The influence of an aligned nanofibrous topography on human mesenchymal stem cell fibrochondrogenesis. Biomaterials. 2010; 31:6190–200. [PubMed: 20494438]
55. Zhang G, et al. Decorin regulates assembly of collagen fibrils and acquisition of biomechanical properties during tendon development. J Cell Biochem. 2006; 98:1436–49. [PubMed: 16518859]
56. Berglund M, Reno C, Hart DA, Wiig M. Patterns of mRNA expression for matrix molecules and growth factors in flexor tendon injury: differences in the regulation between tendon and tendon sheath. J Hand Surg Am. 2006; 31:1279–87. [PubMed: 17027787]
57. Docheva D, Hunziker EB, Fassler R, Brandau O. Tenomodulin is necessary for tenocyte proliferation and tendon maturation. Mol Cell Biol. 2005; 25:699–705. [PubMed: 15632070]
58. Cardwell RD, Dahlgren LA, Goldstein AS. Electrospun fibre diameter, not alignment, affects mesenchymal stem cell differentiation into the tendon/ligament lineage. J Tissue Eng Regen Med. 2014; 8:937–45. [PubMed: 23038413]
59. Erisken C, Zhang X, Moffat KL, Levine WN, Lu HH. Scaffold fiber diameter regulates human tendon fibroblast growth and differentiation. Tissue Eng Part A. 2013; 19:519–28. [PubMed: 23150905]
60. Dayan D, Hiss Y, Hirshberg A, Bubis JJ, Wolman M. Are the polarization colors of picrosirius red-stained collagen determined only by the diameter of the fibers? Histochemistry. 1989; 93:27–9. [PubMed: 2482274]
61. Costa KD, Lee EJ, Holmes JW. Creating alignment and anisotropy in engineered heart tissue: role of boundary conditions in a model three-dimensional culture system. Tissue Eng. 2003; 9:567–77. [PubMed: 13678436]
62. Desai RA, Gao L, Raghavan S, Liu WF, Chen CS. Cell polarity triggered by cell-cell adhesion via E-cadherin. J Cell Sci. 2009; 122:905–11. [PubMed: 19258396]
63. Doxzen K, et al. Guidance of collective cell migration by substrate geometry. Integr Biol (Camb). 2013; 5:1026–35. [PubMed: 23784144]
64. Kolambkar YM, Bajin M, Wojtowicz A, Hutmacher DW, Garcia AJ, Guldberg RE. Nanofiber orientation and surface functionalization modulate human mesenchymal stem cell behavior in vitro. Tissue Eng Part A. 2014; 20:398–409. [PubMed: 24020454]
65. Gilchrist CL, Ruch DS, Little D, Guilak F. Micro-scale and meso-scale architectural cues cooperate and compete to direct aligned tissue formation. Biomaterials. 2014; 35:10015–24. [PubMed: 25263687]
66. Chang JC, Fujita S, Tonami H, Kato K, Iwata H, Hsu SH. Cell orientation and regulation of cell-cell communication in human mesenchymal stem cells on different patterns of electrospun fibers. Biomed Mater. 2013; 8:055002. [PubMed: 24002690]
67. Benhardt HA, Cosgriff-Hernandez EM. The role of mechanical loading in ligament tissue engineering. Tissue Eng Part B Rev. 2009; 15:467–75. [PubMed: 19583461]
68. Hannafin JA, Arnoczky SP, Hoonjan A, Torzilli PA. Effect of stress deprivation and cyclic tensile loading on the material and morphologic properties of canine flexor digitorum profundus tendon: an in vitro study. J Orthop Res. 1995; 13:907–14. [PubMed: 8544028]
69. Lake SP, Miller KS, Elliott DM, Soslowsky LJ. Effect of fiber distribution and realignment on the nonlinear and inhomogeneous mechanical properties of human supraspinatus tendon under longitudinal tensile loading. J Orthop Res. 2009; 27:1596–602. [PubMed: 19544524]
70. Itoi E, Berglund LJ, Grabowski JJ, Schultz FM, Growney ES, Morrey BF, An KN. Tensile properties of the supraspinatus tendon. J Orthop Res. 1995; 13:578–84. [PubMed: 7674074]
71. Aurora A, McCarron J, Iannotti JP, Derwin K. Commercially available extracellular matrix materials for rotator cuff repairs: state of the art and future trends. J Shoulder Elbow Surg. 2007; 16:S171–S8. [PubMed: 17560804]
72. Pitt, CG. Poly-ε-caprolactone and its copolymers. In: Langer, R.; Chasin, M., editors. Biodegradable Polymers as Drug Delivery Systems. New York: Marcel Dekker; 1990. p. 71-120.
73. Engelberg I, Kohn J. Physico-mechanical properties of degradable polymers used in medical applications: a comparative study. Biomaterials. 1991; 12:292–304. [PubMed: 1649646]

74. Chaudhury S, Holland C, Thompson MS, Vollrath F, Carr AJ. Tensile and shear mechanical properties of rotator cuff repair patches. J Shoulder Elbow Surg. 2012; 21:1168–76. [PubMed: 22079767]

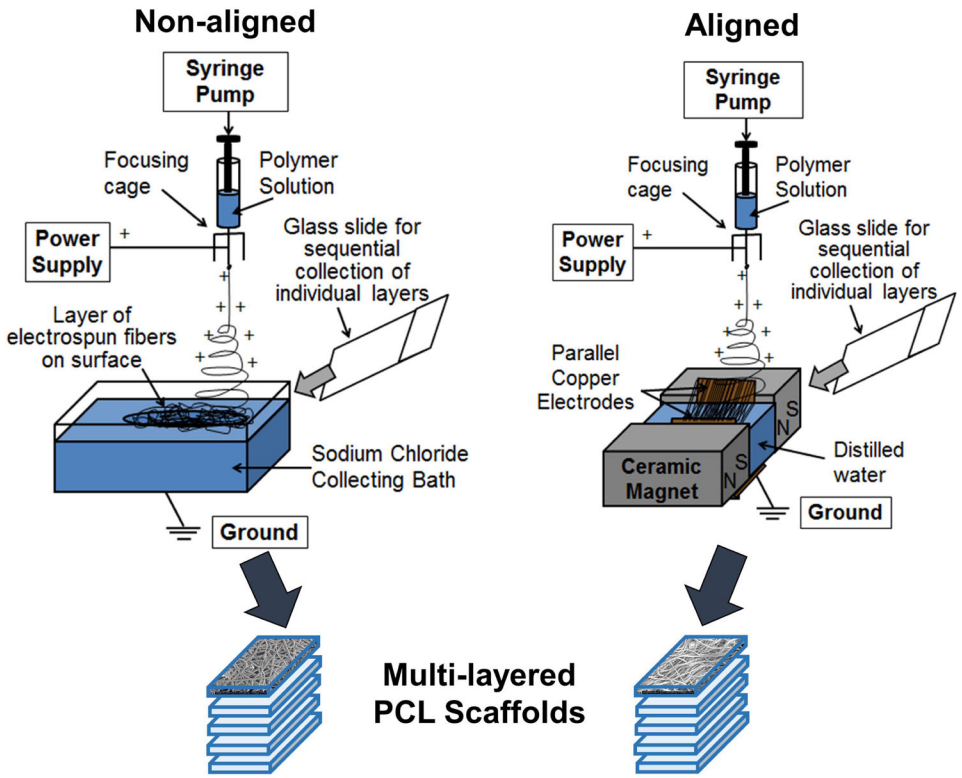

Fig. 1.

Electrospinning apparatus for nonaligned and aligned electrospun scaffolds. Nonaligned layers are collected sequentially from the surface of a grounded saline collecting bath to form multilayered nonaligned scaffolds. Similarly, aligned layers are collected sequentially from between the alignment apparatus to form multi-layered aligned scaffolds.

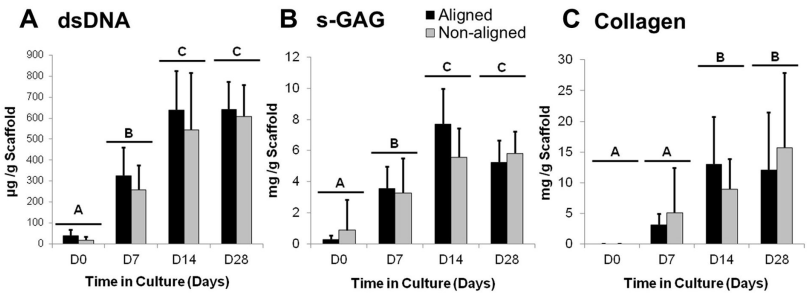

Fig. 2.

Mean dsDNA (A), sulfated glycosaminoglycan (s-GAG) (B), and collagen (C) content of aligned and nonaligned multilayered electrospun poly(ε)caprolactone scaffolds 0, 7, 14, and 28 days after seeding with 0.5×10^6 human adipose-derived stem cells/cm^2. Whiskers indicate standard deviation; n=5 per group. Bars with different letters above are significantly different from each other, $p \leq 0.05$.

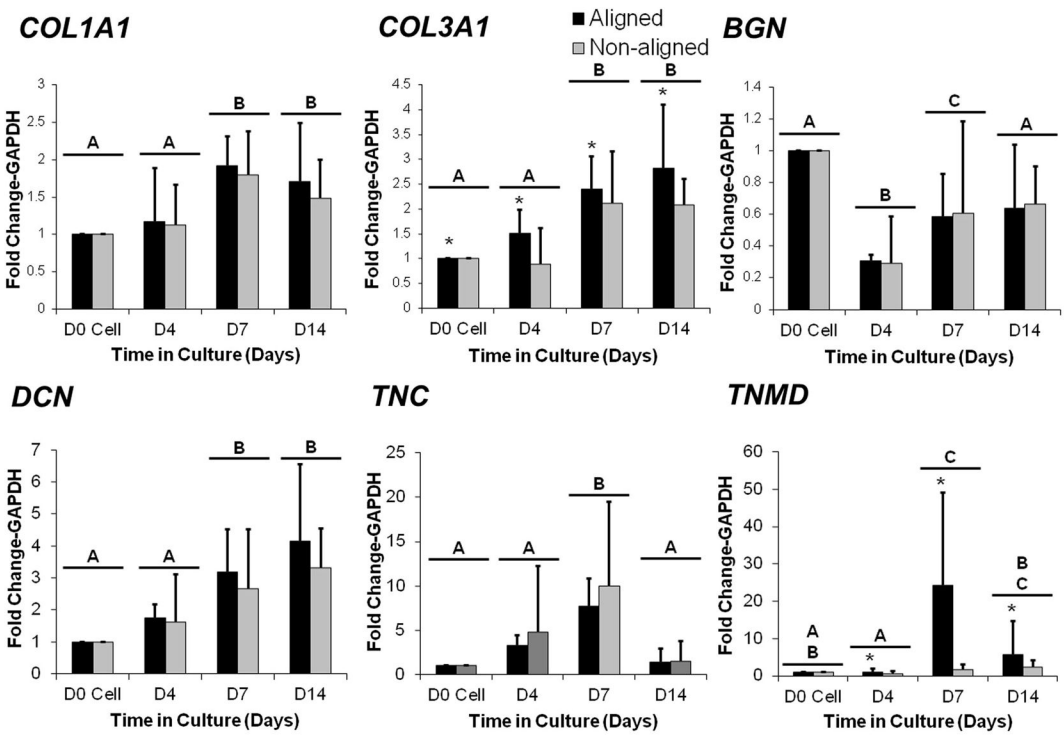

Fig. 3.

Mean gene expression of type I collagen (*COL1A1*), type III collagen (*COL3A1*), biglycan (*BGN*), decorin (*DCN*), tenascin-C (*TNC*), and tenomodulin (*TNMD*) at 7, 14, and 28 days of culture normalized to day 0 and *GAPDH* expression. Whiskers indicate standard deviation; n=5 per group. Bars with different letters above are significantly different from each other, $p \leq 0.05$. *Aligned greater than nonaligned, $p \leq 0.05$.

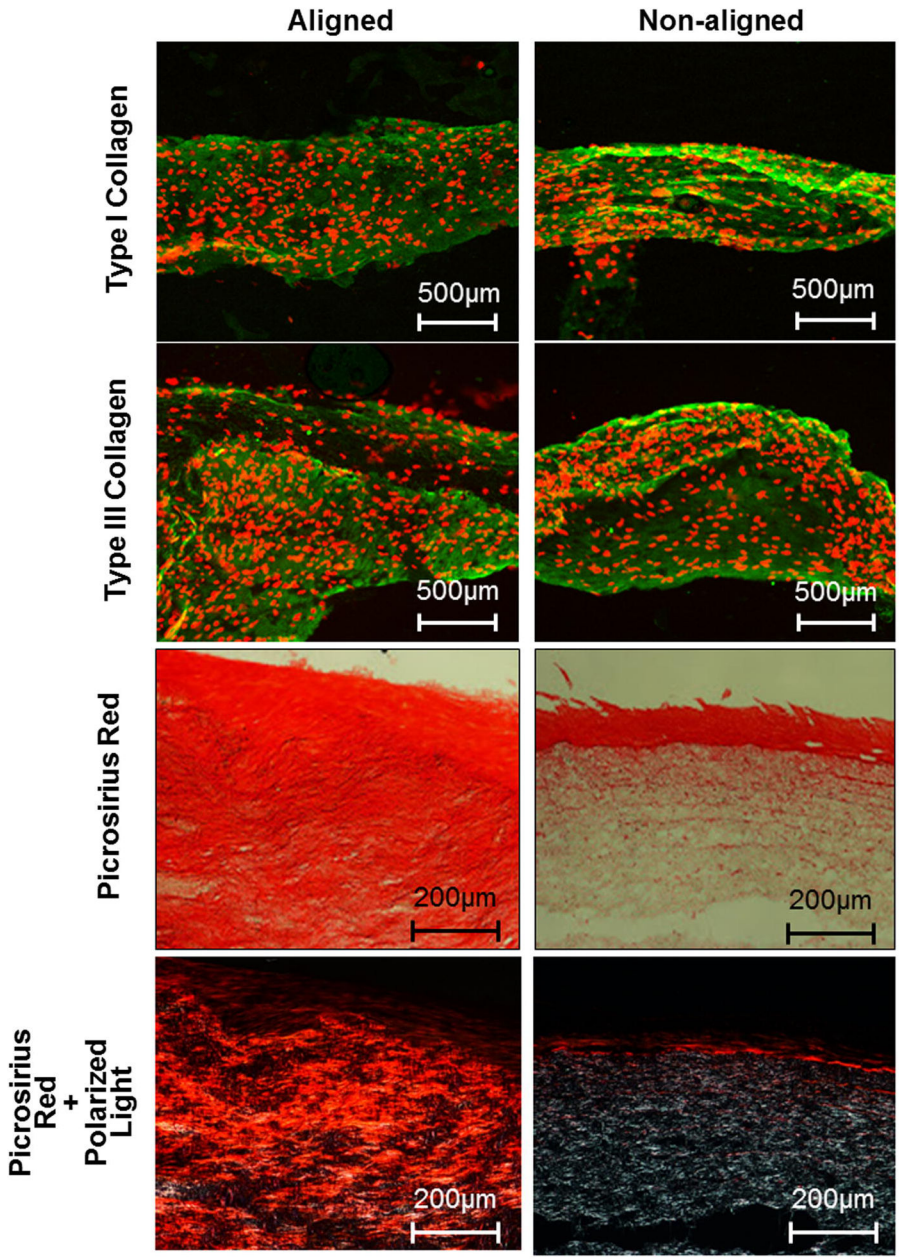

Fig. 4.

Human type I and type III collagen immunofluorescence (fluorescein isothiocyanate; green) with nuclear counterstain (propidium iodide; red), and Picrosirius Red staining under visible and polarized light in aligned and nonaligned hASC-seeded scaffolds cultured for 28 days.

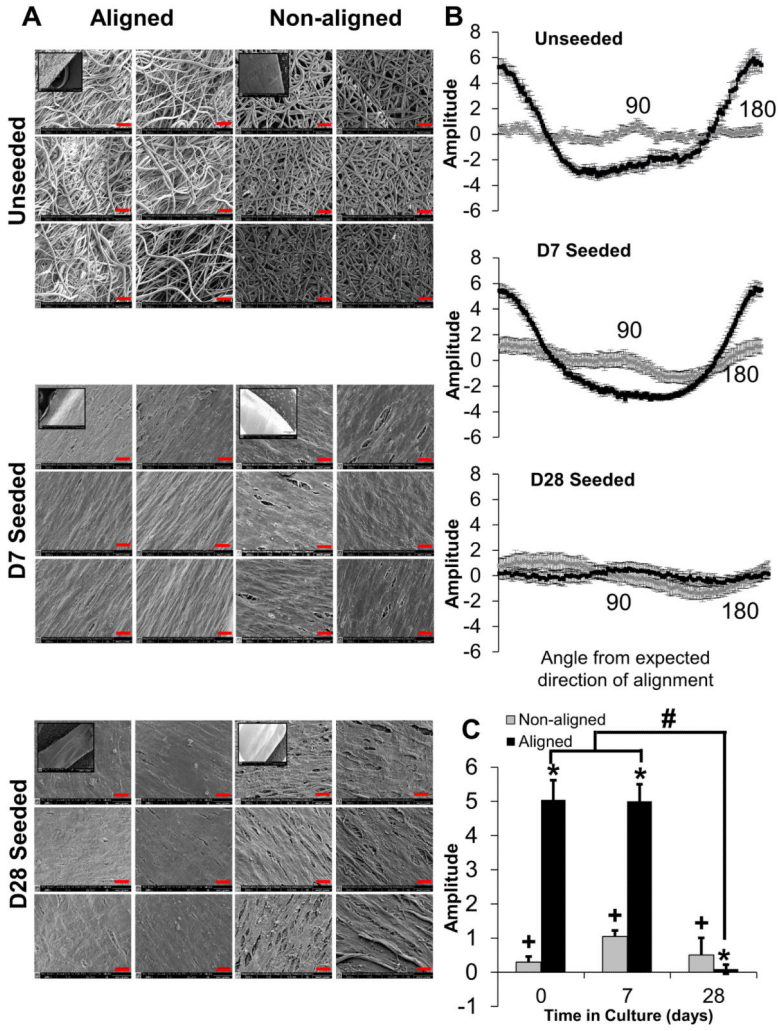

Fig. 5.

Scanning electron micrographs of aligned and nonaligned scaffolds over 28 days in culture (A) Scale bar = 20μm. Inset images represent long axis scaffold border along direction of expected fiber alignment. Fast Fourier transform results (B) of the same scaffolds (*n*=5, 6 images/scaffold), and fiber alignment index (C) of aligned and nonaligned scaffolds. Plus symbol (+) indicates significantly different from other nonaligned bars with the same symbol, asterisk (*) indicates different from nonaligned at same time point, and the hash sign (#) indicates day 0 and 7 different to day 28.

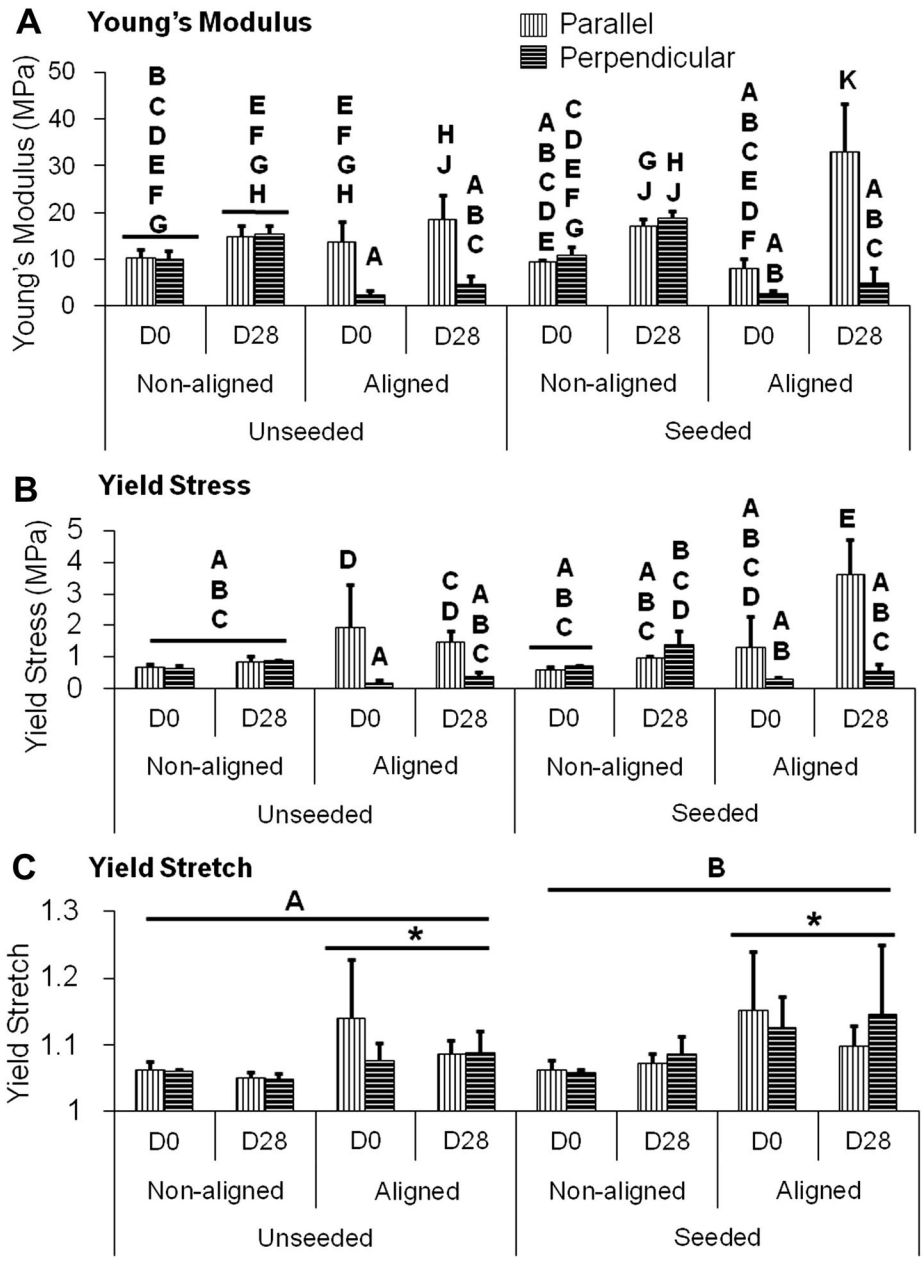

Fig. 6.

Mean Young's modulus (A), yield stress (B), and yield stretch (C) in seeded and unseeded aligned and nonaligned scaffolds tested in orthogonal dimensions after 0 and 28 days of culture. Whiskers indicate standard deviation; n=6. Bars with different letters above are significantly different from each other, $p \leq 0.05$.